Optimal linear growth in spiral Poiseuille flow

C. J. HEATON

Department of Applied Mathematics and Theoretical Physics, University of Cambridge,
Wilberforce Road, Cambridge CB3 0WA, UK

Computations are presented of the optimal linear growth in spiral Poiseuille flow(SPF). The aim is to complement a recent presentation of the complete neutral curves for this flow (Cotrell & Pearlstein, J. Fluid Mech. vol. 509, 2004, p. 331) with a study of the transient growth possible in the stable parameter regions. Maximum growth is computed over the full range of axial and azimuthal wavenumbers for the same three test cases as considered by Cotrell & Pearlstein: radius ratio $\eta = 0.5$ and rotation rate ratio $\mu = -0.5$, 0 and 0.5. A connection is established between two regimes of optimal transients in spiral Poiseuille flow. The first occurs for axial Reynolds number $Re \gg 1$ and Taylor number $Ta = O(1)$, with transient growth of streamwise disturbances analogous to that in non-swirling shear flows. In the second regime $Ta \gg 1$, and we find centrifugal transients of a different type. In this latter regime we obtain the first numerical verification of a recently conjectured scaling for centrifugal transient growth. Our results imply different transition scenarios, triggered by either transient growth or asymptotic instabilities, in the small-Re and large-Re regimes, consistent with previous experimental data. We also study a model for the secondary instability of the optimal transients, as a proposed explanation for the subcritical and delayed transition seen in experiments at moderately large Re. The model is found to favour delayed onset for smaller μ and subcritical onset for larger μ, in good qualitative agreement with the experimental data.

1. Introduction

Spiral Poiseuille flow (SPF) is the steady flow occurring between two concentric cylinders when driven by both differential rotation of the cylinders and an imposed axial pressure gradient. SPF is important in several applications, e.g. in the cooling of rotating machinery and in journal bearing lubrication. It is also a flow of significant theoretical interest because it exhibits both centrifugal and shear instabilities. Following Taylor's (1923) work on rotating flow without an axial component, early work on SPF stability concentrated on axisymmetric disturbances (Goldstein 1937; DiPrima 1960; Chandrasekhar 1962). Theoretical results for non-axisymmetric disturbances were given by Takeuchi & Jankowski (1981), Ng & Turner (1982), and Meseguer & Marques (2002). Recently Cotrell & Pearlstein (2004) and Meseguer & Marques (2005) have given complete linear stability boundaries up to Reynolds number $Re = O(10^4)$. A full review of the history of SPF stability is given by Cotrell & Pearlstein (2004).

1.1. *Motivation*

The present work is motivated by the work of Cotrell & Pearlstein (2004), who present the complete neutral curves for linear stability of SPF, and the companion paper by

Cotrell, Rani & Pearlstein (2004), in which the theoretical results are compared to the available experimental data. Cotrell & Pearlstein's neutral curves are described as *complete* because they include both Tollmien–Schlichting (shear) instabilities, which determine the neutral curve at large Re, and the centrifugal instabilities which are prevalent at smaller Re. The existence of Tollmien–Schlichting instabilities at high Re in SPF was conjectured by Reid (1961), and their confirmation by Cotrell & Pearlstein (2004) and Meseguer & Marques (2005) is a significant step forward in the context of SPF stability theory. However, the neutral curve of any large-Re shear flow, and particularly one with Tollmien–Schlichting instabilities, immediately raises a further question: what direct significance do the instabilities have? There has been strong interest in recent years in the so-called bypass transition to turbulence of parallel shear flows (Schmid & Henningson 2001), and it is now widely accepted that Tollmien–Schlichting waves do not play a direct role in some transition scenarios. Instead, the starting point for bypass transition mechanisms is generally linear *transient* growth. With this in mind, it is naturally desirable to map the levels of optimal transient growth in order to gain further insight into the stability of SPF. If transient growth levels are low then this supports the idea that transition should occur at the neutral curve, whereas if transient growth is particularly strong bypass transition may become a possibility, in which case the neutral curve may not then dictate transition. A lesson from the transition studies of parallel flows is that computations of transient growth can contribute information on the meaning of the neutral curve for transition; therefore this gives strong theoretical motivation for the present investigation.

Various experiments on SPF stability have been performed, and are comprehensively reviewed by Cotrell *et al.* (2004). They compared the values of Ta_{crit}^{expt}, the critical value of the Taylor number Ta at which transition was observed experimentally, with Ta_{crit}^{theo}, the critical Ta on the theoretical neutral curve. A brief summary of the comparison is that excellent agreement is generally obtained for small Re. However for large Re the agreement is poor, with Ta_{crit}^{expt} decreasing to zero at $Re = O(10^3)$ while Ta_{crit}^{theo} is non-zero and approximately independent of Re in this range. In an intermediate range $200 \lesssim Re \lesssim 400$, a relatively small systematic difference between Ta_{crit}^{expt} and Ta_{crit}^{theo} is found. These broad trends tend to support a hypothesis that for small Re transition occurs at the neutral curve, whereas for large Re a bypass transition occurs which does not involve the instability modes. For $Re \gg Ta$ the flow is approximately annular Poiseuille flow, with only a very small rotation, so experimental transition to turbulence at $Re = O(10^3)$ is unsurprising. Assuming that the transition of (annular) Poiseuille flow follows a bypass mechanism reliant on transient growth, then one is lead to speculate that at large Re transient growth effects are the dominant linear growth mechanism in SPF, but that at small Re they are a small and unimportant effect. Hence the experimental evidence motivates an investigation of the transient growth in SPF in order to test this hypothesis.

1.2. *Transient growth*

The phenomenon of transient growth results from the fact that, for any non-trivial mean flow, the linearized Navier–Stokes equations correspond to a non-normal operator. In a non-normal linear system transient growth can occur at short times, even if the system is stable and all signals decay at large times. For this reason transient growth has frequently been studied as a means of growth in parallel shear flows (Gustavsson 1991; Butler & Farrell 1992; Trefethen *et al.* 1993; Schmid & Henningson 1994) and more recently has also been applied to vortex-type shear flows (Antkowiak & Brancher 2004; Pradeep & Hussain 2006; Antkowiak & Brancher

2007; Heaton & Peake 2007; Heaton 2007). Transient growth is quantified by taking the initial-value problem of the linearized Navier–Stokes equations and finding the maximum possible growth, as measured by kinetic energy, with the maximum being taken over all possible initial conditions. The initial condition corresponding to maximal growth is known as the optimal perturbation. The numerical calculation of optimal transients can be performed by a variety of methods; in this paper we will follow the method of Schmid & Henningson (2001), as will be fully described below.

The transient growth possible in SPF will be computed for the same three representative test cases used by Cotrell & Pearlstein (2004) in their calculations of the neutral curve. These cases have radius ratio $\eta = 0.5$ and rotation rate ratio (of the outer and inner cylinders) $\mu = 0, \pm 0.5$. It is possible to extrapolate from these test cases, at least in a qualitative manner, to other cases such as small radius ratio (Cotrell & Pearlstein 2006), narrow gap, etc. Transient growth has been computed in Taylor–Couette flow by Hristova *et al.* (2002) and Meseguer (2002), but we are not aware of any previous studies of transient growth in SPF. For the three test cases we compute the maximum transient growth, maximized over time and over all wavenumbers, throughout the stable portion of the (Re, Ta)-plane. For large Re and fixed Ta we find transients characteristic of a nearly parallel shear flow with a streamwise-independent structure. In the alternative limit of large Re and large Ta (which is stable only when $\mu > \eta^2$) we recover a different type of transient, which we refer to as centrifugal, characteristic in flow with comparable swirl and axial velocity. The centrifugal transients have recently been investigated by Heaton & Peake (2007), who present scalings and a mathematical treatment which differ from those for parallel shear flows (Schmid & Henningson 2001). An interesting aspect of our results is the ability to connect two regimes consisting of these two different types of transient growth in different parts of the (Re, Ta)-plane for SPF – this result is in the same spirit as the connection recently found between centrifugal and Tollmien–Schlichting asymptotic instabilities in SPF. For the centrifugal transients one particular result is that we are able to directly confirm the scalings given by Heaton & Peake (2007) for the magnitude of the transient growth. The scaling $G \sim Re^{(2+2\sigma)/3}$ (where G is the growth and σ an exponent defined below) was not possible to observe with the numerical method employed by Heaton & Peake (2007). Here we are able to observe and confirm this scaling law for the first time.

On comparison to the experimental data reviewed by Cotrell *et al.* (2004) and the neutral curves of Cotrell & Pearlstein (2004), our transient growth results will support the scenario suggested in §1.1: for the small-Re experimental data transient growth is weak, consistent with transition occurring via classical centrifugal instability modes. Contrastingly, at large Re transient growth is large and consistent with the bypass transition of Poiseuille pipe flow. Over the intermediate range $200 \lesssim Re \lesssim 400$ there are experimental data showing small systematic differences from Ta_{crit}^{theo}, the critical value of Ta predicted by the neutral curve. In this regime, which is intermediate between modal- and transient-dominated regimes, we will propose an explanation for the data in which both effects are present. Using Floquet theory the secondary effect of the transients on the primary mode is studied, and this model is found to recover the correct qualitative trend for subcritical and delayed onset.

The remainder of this paper is organized as follows. In §2 we formulate the stability problem and describe our numerical method. In §3 we give our results for the transient growth in SPF, and discuss the relationship to both experimental data and previous studies of asymptotic instability in SPF. In §4 we propose a model for the subcritical and delayed transition seen in some experiments. Final conclusions are given in §5.

2. Problem formulation

Incompressible fluid is considered, confined between two coaxial rotating cylinders and driven by a constant axial pressure gradient. We work in cylindrical polar coordinates (x, r, θ) aligned with the axis of the cylinders. We follow the formulation adopted by Takeuchi & Jankowski (1981), Ng & Turner (1982) and Cotrell & Pearlstein (2004). The problem is non-dimensionalized by scaling lengths with the difference between the cylinder radii, scaling velocities with the averaged axial velocity, and scaling densities with the constant fluid density.

The flow is thus confined between $r = \eta/(1 - \eta)$ and $r = 1/(1 - \eta)$, where $\eta < 1$ is the radius ratio of the cylinders. The steady mean flow is SPF and is given by

$$U(r) = 2\frac{(1 - r^2(1 - \eta)^2)\log \eta - (1 - \eta^2)\log(r(1 - \eta))}{1 - \eta^2 + (1 + \eta^2)\log \eta}, \tag{2.1}$$

$$V(r) = 0, \tag{2.2}$$

$$W(r) = \frac{Ta}{Re}\left(\frac{r(\mu - \eta^2)}{1 - \eta^2} + \frac{\eta^2(1 - \mu)}{r(1 - \eta)^3(1 + \eta)}\right), \tag{2.3}$$

where μ is the ratio of the angular velocities of the outer and inner cylinders, Re is the Reynolds number based on the average axial flow and Ta is the Taylor number based on the rotation rate of the inner cylinder. In terms of dimensional quantities,

$$\eta = R_i/R_o, \quad \mu = \Omega_o/\Omega_i, \quad Re = \overline{U}(R_o - R_i)/\nu, \quad Ta = \Omega_i(R_o - R_i)^2/\nu, \tag{2.4}$$

where R_i, R_o, $\overline{U}$, Ω_i, Ω_o and ν are respectively the dimensional values of: the inner and outer cylinder radii, the mean axial speed, the inner and outer cylinder angular velocities and the kinematic viscosity.

The stability problem for SPF is characterized by the four quantities η, μ, Re, and Ta. SPF exhibits both shear and centrifugal behaviour: annular Poiseuille flow is recovered in the limit $Ta/Re \ll 1$, circular Couette flow is recovered when $Ta/Re \gg 1$. For $Ta/Re = O(1)$ SPF combines both in a swirling jet-type flow. The narrow-gap limit, considered by Hristova *et al.* (2002) for example, corresponds to $\eta \to 1$.

2.1. Stability equations

The mean flow (2.1)–(2.3) is perturbed by a velocity disturbance $(u, v, w)e^{im\theta + ikx}$ and pressure disturbance $pe^{im\theta + ikx}$. We take m and k to be real wavenumbers, with m an integer, and the complex amplitudes u, v, w and p are functions of time t and radius r. The linearized Navier–Stokes equations become

$$\frac{\partial u}{\partial t} + \chi iu + vU' = -ikp + Re^{-1}\left[\frac{(ru')'}{r} - \left(\frac{m^2}{r^2} + k^2\right)u\right], \tag{2.5}$$

$$\frac{\partial v}{\partial t} + \chi iv - \frac{2Ww}{r} = -p' + Re^{-1}\left[\frac{(rv')'}{r} - \left(\frac{1 + m^2}{r^2} + k^2\right)v - \frac{2imw}{r^2}\right], \tag{2.6}$$

$$\frac{\partial w}{\partial t} + \chi iw + \frac{(Wr)'v}{r} = -\frac{imp}{r} + Re^{-1}\left[\frac{(rw')'}{r} - \left(\frac{1 + m^2}{r^2} + k^2\right)w + \frac{2imv}{r^2}\right], \tag{2.7}$$

$$0 = iku + \frac{(rv)'}{r} + \frac{imw}{r}, \tag{2.8}$$

where $\chi = Uk + Wm/r$ and a prime denotes differentiation with respect to r. The boundary conditions on the disturbance velocity are no slip on the cylinders, i.e. $u = v = w = 0$ at $r = \eta/(1 - \eta), 1/(1 - \eta)$.

Equations (2.5)–(2.8) are solved numerically as described below to find the maximum transient growth. This requires the definition of a norm to measure the growth of the disturbance, for which we use the kinetic energy

$$E(t) = \int_{\eta/(1-\eta)}^{1/(1-\eta)} \tfrac{1}{2}(|u|^2 + |v|^2 + |w|^2) r \, \mathrm{dr}. \qquad (2.9)$$

Using the energy norm (2.9), we define the energy amplification at a given time and for a given initial condition as $E(t)/E(0)$. We wish to maximize this quantity over all initial conditions, $\boldsymbol{u}(t=0)$. The maximum energy amplification at a given time is called the *gain* $G(t)$. The gain curve $G(t)$ provides an envelope for all possible curves of energy amplification. For cases of SPF which are stable all disturbances decay at long times, so it is conventional to define the maximum gain

$$G_{max} = \max_t \ G(t), \qquad (2.10)$$

with t_{max} denoting the time at which the maximum is attained. The quantity G_{max} still depends on the wavenumbers, so we further define

$$\mathbb{G} = \max_{m,k} \ G_{max}, \qquad (2.11)$$

where $\mathbb{G} = \mathbb{G}(\eta, \mu, Ta, Re)$ depends only on the properties of the mean flow. The disturbance whose energy amplification is maximal and attains the gain $\mathbb{G}$ is known as the optimal disturbance.

The quantities given by (2.10)–(2.11) are the most commonly used measure of transient growth levels. We shall use (2.10)–(2.11) in the rest of this paper, but note that by using them we are restricted to considering asymptotically stable configurations only. We note that transient growth over a finite time interval could be important even in an asymptotically unstable flow, but this would require a different analysis and is not considered here.

2.2. Numerical method

In order to compute the gain $G(t)$ we first discretize the spatial radial coordinate in (2.5)–(2.8) using a pseudospectral collocation technique. Using N collocation points for this discretization, equations (2.5)–(2.8) are transformed into a $(4N \times 4N)$ matrix equation. The gain is then calculated using the method described in Chapter 4 of Schmid & Henningson (2001). First the frequency eigenvalues and eigenvectors of (2.5)–(2.8) are found by assuming time dependence of the form $\exp(-i\omega t)$, and then solving the eigenvalue problem in the discretized matrix form of the equations. The eigenvalue ω with the greatest imaginary part (i.e. growth rate) is the primary eigenvalue and its associated eigenvector is the primary mode. The stability of the primary mode was the subject of the study by Cotrell & Pearlstein (2004) and previous authors, and determines the long-time asymptotic linear stability of SPF. To determine the transient behaviour over finite times, however, requires knowledge of all the modes in the spectrum (Trefethen *et al.* 1993). The matrix equation is diagonalized using the basis of eigenvectors, so that the temporal evolution of disturbances according to (2.5)–(2.8) is given by a simple matrix exponential. The maximum gain is then computed as the norm of the matrix exponential, where the appropriate norm is dictated by (2.9); see Schmid & Henningson (2001) for full details. We use MATLAB$^{\text{TM}}$ to perform the linear algebra on a standard desktop computer. The limiting step in the calculation of the gain is the eigenvalue-eigenvector calculation which has $O(N^3)$ complexity. In most cases we find that $N = 20$ is sufficient to eliminate truncation

error and obtain satisfactory convergence. The Tollmien–Schlichting modes however require more collocation points, $N = 35$ being found to be sufficient.

The gain $G(t)$ can be maximized over t without having to repeat the eigenvalue-eigenvector calculation, and hence each value of G_{max} is a relatively fast and straightforward calculation. However, maximizing over the two remaining variables m and k to obtain $\mathbb{G}$ increases the length of the computation significantly. A small saving is possible because the gain is invariant under the transformation $(m, k) \rightarrow (-m, -k)$, so we may restrict to $m \geqslant 0$ without loss of generality. The maximization over m and k was performed by taking each value of m in turn and maximizing over k with a simple bisection procedure, terminating when the relative error in the gain was less than 1%. It is important to ensure that a sufficiently wide range of m and k is included in order to obtain the correct maximum gain $\mathbb{G}$. This had to be checked manually in a representative subset of cases for each computation. Note that a consequence of the method used is that the maximum gain $\mathbb{G}$ is found to 1% relative error, but the axial wavenumber at the maximum, k_{max}, is not. Our results include many cases in which k_{max} is close to zero, for which the relative error in the calculated value of k_{max} is therefore large. We do not therefore give detailed plots of k_{max}, as this would have necessitated more stringent tolerances and slower computations than are required to find $\mathbb{G}$.

Our code is validated by comparing results for the primary mode with Cotrell & Pearlstein (2004), who in turn have validated their results against several previous authors' calculations. We obtain excellent agreement with the results in figures 1,2 and 4 of Cotrell & Pearlstein (2004) describing the neutral curve for $\eta = 0.5$ and $\mu = 0, \pm 0.5$. The neutral curves we calculate are included in the figures below as thick black lines. When superimposed on the figures of Cotrell & Pearlstein (2004) there is no visible difference, so we conclude that our code is obtaining the correct eigenvalues and eigenvectors. The remainder of the code, which takes the spectrum information and finds the maximum gain, is a standard routine. This was tested by comparing to the test case Meseguer (2002) used for Taylor–Couette flow, which in our definitions is $\eta = 0.881$, $\mu = -1$, $Re = 0$, $Ta = 32.42$, $m = 0$, $k = \pi$. We calculate $G_{max} = 16.62$ for this test case, in agreement with Meseguer (2002) and Hristova et al. (2002).

3. Transient growth in SPF

We report the results of our transient growth calculations in this section. The same three test cases for which Cotrell & Pearlstein (2004) gave the full neutral curves are chosen, so that the relationship between transient growth and asymptotic stability can be studied. In each case the maximum gain $\mathbb{G}$ is presented throughout the stable region of the (Re, Ta)-plane. The radius ratio is $\eta = 0.5$ throughout this section.

3.1. Stationary outer cylinder ($\mu = 0$)

We consider first the case of a stationary outer cylinder, $\mu = 0$. The stable region for this case is the finite region of the (Re, Ta)-plane in figure 1 below the neutral curve, shown by a thick black line. As mentioned in §2.2, the neutral curve we find has been checked against that of Cotrell & Pearlstein (2004) as part of the validation of our numerical code. The scalloped nature of the neutral curve is due to integer jumps in m_{crit}, the azimuthal wavenumber of the primary mode on the neutral curve. Figure 1 shows the contours of maximum transient growth $\mathbb{G}$ and figure 2 shows the azimuthal wavenumber m_{max} at which the growth is attained. Note that since m_{max} only takes
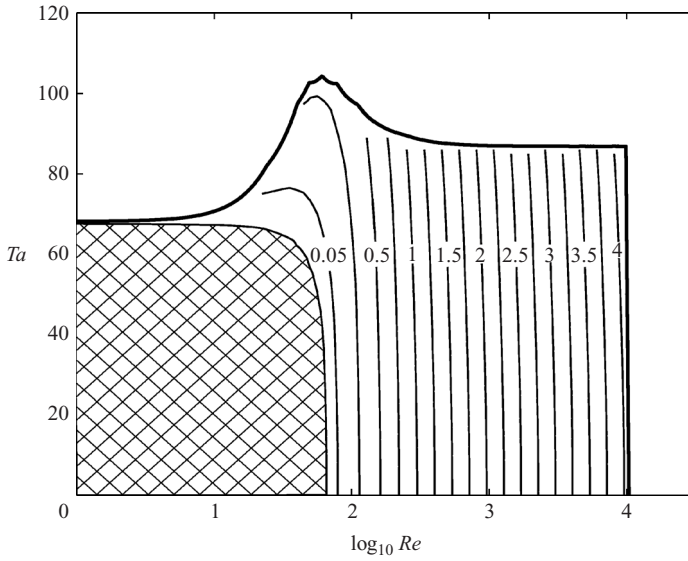
FIGURE 1. Contours of maximum transient growth $\mathbb{G}$ for $\eta = 0.5$, $\mu = 0$. Contour labels show the value of $\log_{10} \mathbb{G}$, in steps of 0.25 unless otherwise indicated. The thick line is the neutral curve for asymptotic linear stability. $\mathbb{G} \equiv 1$ throughout the hatched region.
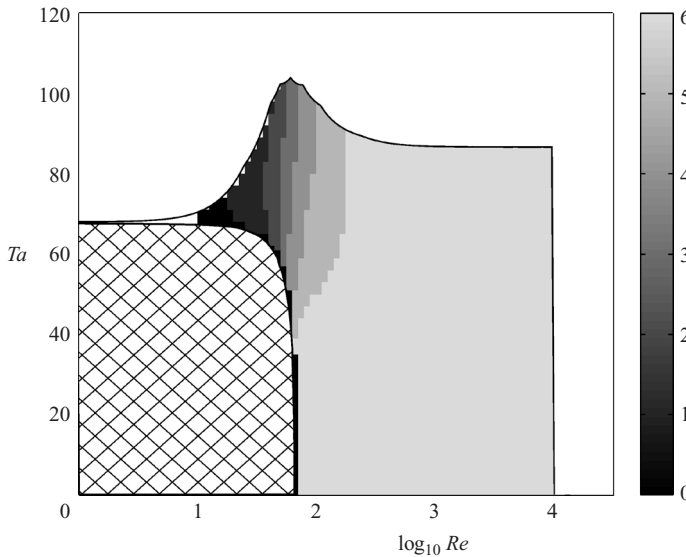

FIGURE 2. Values of m which attain the maximum transient growth for $\eta = 0.5$, $\mu = 0$.

discrete values, the shaded plot in figure 2 inevitably appears more coarsely resolved than the plot of $\mathbb{G}$ in figure 1, but the same grid was used to produce both plots.

For low Re there is a large area in which $\mathbb{G} \equiv 1$, meaning that no growth whatsoever is possible for disturbances governed by the linearized equations. In this region all disturbances decay monotonically, so the time of the maximum growth is trivially $t_{max} = 0$ and the azimuthaly wavenumber m_{max} is undefined. Where transient growth is possible, it is found that m_{max} generally increases with Re, starting from $m_{max} = 0$

at $Re = 0$. A similar trend was observed in m_{crit} along the neutral curve (see Cotrell & Pearlstein 2004, figure 1*b*), although note that the two quantities are different and take different values in places. The boundary of the no-growth region extends from $Ta = 0$, $Re = 66.0$ at one end up to $Ta = 68.2$, $Re = 0$, where it meets the end point of the linear stability boundary (first calculated by DiPrima & Swinney 1985, for Taylor–Couette flow). At $Re = 0$, there is therefore a sharp changeover, as Ta increases, from monotonic decay of all disturbances to instability and unbounded exponential growth. For non-zero values of $Re \leqslant 100$ a rapid changeover from very small maximum growth ($\mathbb{G} \simeq 1$) to linear instability and unbounded exponential growth is still evident. Since there is no linear growth mechanism other than the primary unstable mode which is strong enough to have a significant effect, these results suggest Ta_{crit}^{theo}, the value of Ta on the neutral curve, should give the correct prediction for transition. In their evaluation of several sets of experimental data for the $\mu = 0$ case, Cotrell *et al.* (2004) find that there is generally very good agreement of Ta_{crit}^{theo} with Ta_{crit}^{expt} at small Re, consistent with this conclusion.

For Re increasing beyond 100 the maximum transient growth rapidly increases, up to a maximum of $\mathbb{G} \simeq 10^4$ at the near-vertical portion of the neutral curve, which corresponds to instability of the Tollmien–Schlichting shear mode. The transient growth has $m_{max} = 6$ for all large Re, whereas the Tollmien–Schlichting wave which destabilizes first as Re increases has $m_{crit} = 2$, and hence the two cannot share the same mechanism. In fact the optimal transients in this region have small axial wavenumbers k_{max} and are utilizing the growth mechanism described by Schmid & Henningson (1994) for Hagen–Poiseuille flow. Examination of the data for k_{max} (not plotted) reveals that for $Re \geqslant 400$ there is a very clear and distinct scaling $k_{max} \propto Ta/Re$. When $Ta = 0$ and the SPF becomes annular Poiseuille flow this corresponds to the growth of streamwise rolls into streamwise streaks as found by Schmid & Henningson (1994) and others. For $Ta > 0$ the mean swirl of order $O(Ta/Re)$ causes a small modification in the alignment of streamwise disturbances, and hence this is the scaling for k_{max}. It can be seen in figure 1 that for large Re the maximum transient growth scales as $\mathbb{G} \propto Re^2$, the same as for non-swirling parallel shear flows. For large Re the growth $\mathbb{G}$ is also almost independent of Ta, in contrast to the situation at small Re described above when it is almost independent of Re.

Figure 3 shows the visualization of an example optimal disturbance in the large-Re regime described. For the case shown the energy gain is $\mathbb{G} = 11184$, with $m_{max} = 6$ and $k_{max} = 0.061$. Initially the disturbance is dominated by the radial and azimuthal velocity components v and w, and the axial component u is negligible. This can be quantified by noting the partitioning of the kinetic energy: at $t = 0$ we find that 44% of the kinetic energy is due to v, 56% is due to w and only 0.03% is due to u. Therefore the initial disturbance is predominantly the field in figure 3(*a*), and since the axial wavenumber is small this indeed consists of streamwise rolls. When the disturbance reaches its maximum amplitude at $t = t_{max}$ the kinetic energy is larger by a factor of $\mathbb{G} = 1184$, and of this we find that 99.96% is due to the axial velocity u. Thus the final disturbance is predominantly the field shown in figure 3(*d*), and consists of streamwise streaks.

To summarize, at large Re the main result is that disturbances to SPF experience strong transient growth analogous to that in Hagen–Poiseuille flow, and therefore the linear problem should favour bypass transition to turbulence instead of transition due to linear instability modes. This interpretation is in agreement with the experimental data, which consistently find that Ta_{crit}^{expt} decreases to zero at a value of Re of order 10^3 (Kaye & Elgar 1958; Yamada 1962; Cotrell *et al.* 2004). The transient growth $\mathbb{G}$
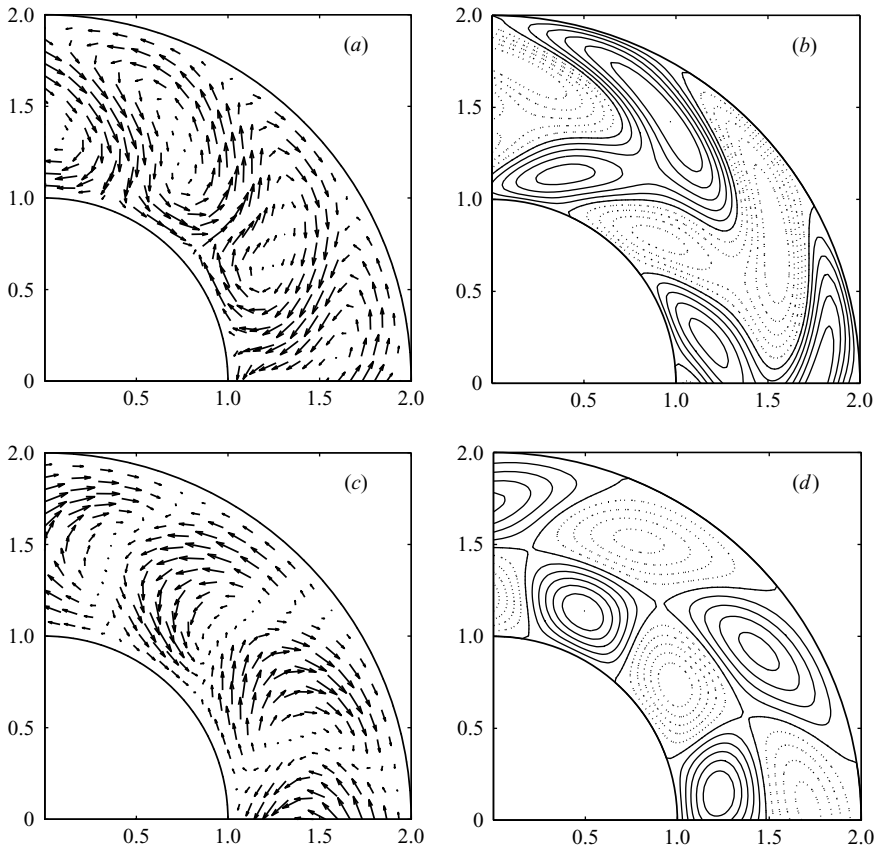
FIGURE 3. Visualizations of the optimal disturbance for $\eta = 0.5$, $\mu = 0$, $Re = 10^{3.5}$, $Ta = 40$. (a, b) $t = 0$, (c, d) $t = t_{max}$. Arrows, (a, c) indicate the cross-section velocity. Contours, (b, d), indicate levels of the axial velocity, with dotted contour lines representing negative values.

therefore explains why the location of the neutral curve, and especially the Tollmien–Schlichting waves, does not play a direct role in experimental realizations of SPF at large Re.

3.2. *Co-rotating outer cylinder* ($\mu = 0.5$)

The maximum transient growth for the case of co-rotating cylinders with $\mu = 0.5$ is given in figure 4, with the corresponding values of m_{max} given in figure 5. Because $\mu > \eta^2$ in this case, the entire $Re = 0$ axis is asymptotically stable (Synge 1938). As a result, the topology of the neutral curve is different to before, with Cotrell & Pearlstein (2004) finding that the neutral curve has two branches for $Re > 70.2$. The lower branch is analogous to the plateau-like neutral curve for $\mu < \eta^2$ (such as $\mu = 0$ discussed above), and extends up to the Re at which the Tollmien–Schlichting wave destabilizes. The upper branch follows a different pattern, with m_{crit} becoming increasingly negative as Re and Ta increase. Calculations are increasingly difficult to perform at large Re and Ta because more basis functions are needed to resolve the eigenmodes, and as a result Cotrell & Pearlstein (2004, p. 345), state that "it is unclear whether the upper branch exists for all Re or has a vertical asymptote". Our computations, like theirs, are not able to determine this matter conclusively; however we note in passing that a plausible explanation for the upper neutral curve is offered by
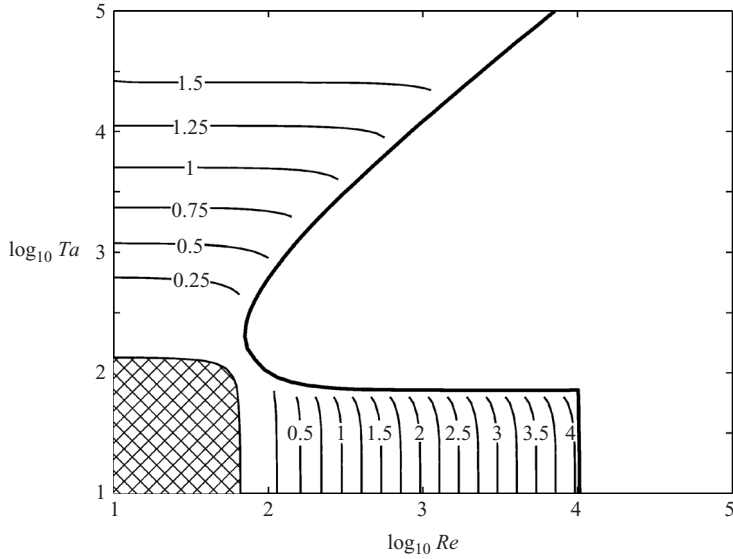
FIGURE 4. Contours of maximum transient growth $\mathbb{G}$ for $\eta = 0.5$, $\mu = 0.5$. Contour labels show the value of $\log_{10} \mathbb{G}$, in steps of 0.25. The thick line is the neutral curve for asymptotic linear stability. $\mathbb{G} \equiv 1$ throughout the hatched region.
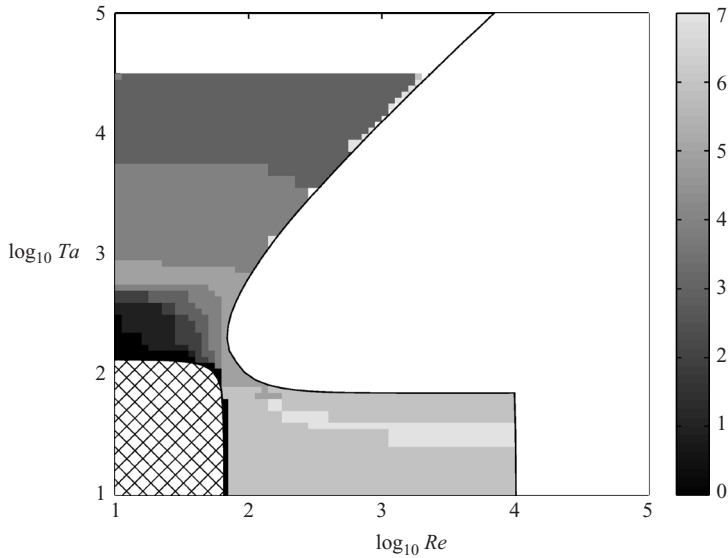

FIGURE 5. Values of m which attain the maximum transient growth for $\eta = 0.5$, $\mu = 0.5$.

the theory of Leibovich & Stewartson (1983), who described inviscid instability modes in swirling flow with $|m|$ asymptotically large and $k = O(|m|)$. Leibovich & Stewartson's theory is applicable here because m_{crit} and k_{crit} both increase with Re along the upper branch (see Cotrell & Pearlstein 2004, figure 2b,c). The stability criterion of Leibovich & Stewartson (1983), when applied to SPF, implies an asymptotic neutral curve as

$Re \to \infty$ of

$$\frac{Ta}{Re} = \frac{(1 - \eta)^2(1 + \eta)(1 - \eta^2 + 2\log\eta)}{\eta\sqrt{(\mu - \eta^2)(1 - \mu)}(1 - \eta^2 + (1 + \eta^2)\log\eta)}. \tag{3.1}$$

For $\eta = \mu = 0.5$ this gives $Ta/Re = 11.59$. The upper branch of the neutral curve in figure 2(a) of Cotrell & Pearlstein (2004) and figure 4 here has $Ta/Re = 12.3$ at $Re = 10^3$, which is in reasonably good agreement. At $Re = 10^4$ in figure 4, $Ta/Re = 14.3$ and the agreement is slightly worse. The shape of the neutral curve suggests that this value will decrease slightly as Re continues to increase but this is beyond the limitations of our computations: we conclude that the curve is consistent with (3.1), but that there is not conclusive proof. We also note that the singularity of (3.1) when $\mu = 1$ is consistent with the numerical discovery (Meseguer & Marques 2002; Cotrell & Pearlstein 2004) of a vertical asymptote in the special case $\mu = 1$.

Turning to the results for the transient growth in figure 4, let us first discuss the trends at smaller Ta. As before, we find a region in which $\mathbb{G} \equiv 1$ and no growth whatsoever is possible in the lower left corner of the plane. For larger Re beneath the lower branch of the neutral curve there is strong transient growth which has the same qualitative features as for the $\mu = 0$ case. The maximum growth visibly scales as $\mathbb{G} \propto Re^2$ and we again have confirmed that the axial wavelength of the optimal disturbances scales as $k_{max} \propto Ta/Re$. The optimal transient has $k_{max} < 0$ in the region of figure 5 below the stripe of $m_{max} = 7$, but this does not affect the transient growth scaling or mechanism. As before we infer that SPF will favour a bypass transition to turbulence in this parameter regime analogous to Hagen–Poiseuille flow, and that the Tollmien–Schlichting waves will not participate. We are not aware of any experimental data at $Re = O(10^3)$ for $\mu \neq 0$, but the strong similarity between the theoretical picture (i.e. the nature of both the neutral curve and the transient growth) and that for $\mu = 0$ suggests that a similar bypass transition will occur.

Strong transient growth is also seen for larger Ta, above both the no-growth region and the upper branch of the neutral curve. In this region the SPF has significant swirl, and the growth evidently has a different character to the streamwise streaks found below the lower branch where the swirl is weak. At larger Ta it is appropriate to apply the results of Heaton & Peake (2007), who described the transient growth in swirling flows in terms of the underlying inviscid algebraic instability (Heaton & Peake 2006). The two distinct limits to consider are $Re \to \infty$ with Ta/Re held fixed, and $Ta \to \infty$ with Re held fixed. In the former limit the mean flow (2.1)–(2.3) is a fixed combination of swirl and axial flow, so the results of Heaton & Peake (2007) should apply directly. In the latter limit the mean flow is instead purely rotational, but the results of Heaton & Peake (2007) can still be applied.

In the limit $Re \to \infty$ with Ta/Re held fixed, Heaton & Peake (2007) derive the following scaling for the transient growth for given wavenumbers m, k:

$$G_{max} \sim Re^{(2+2\sigma)/3}, \quad t_{max} \sim Re^{1/3}. \tag{3.2}$$

The exponent σ is the exponent of an underlying algebraic instability to which inviscid swirling flows are susceptible (Heaton & Peake 2006), and is given by

$$\sigma = \max_r \ \text{Re}\left(-\frac{1}{2} + \sqrt{\frac{1}{4} - \frac{2Wk(k(Wr)' - mU')}{r^2(m(W/r)' + kU')^2}}\right). \tag{3.3}$$

In (3.3) Re(−) denotes the real part, r takes the values $\eta/(1 - \eta) \leqslant r \leqslant 1/(1 - \eta)$ corresponding to the radii in the annulus, while U and W are given by (2.1) and (2.3).
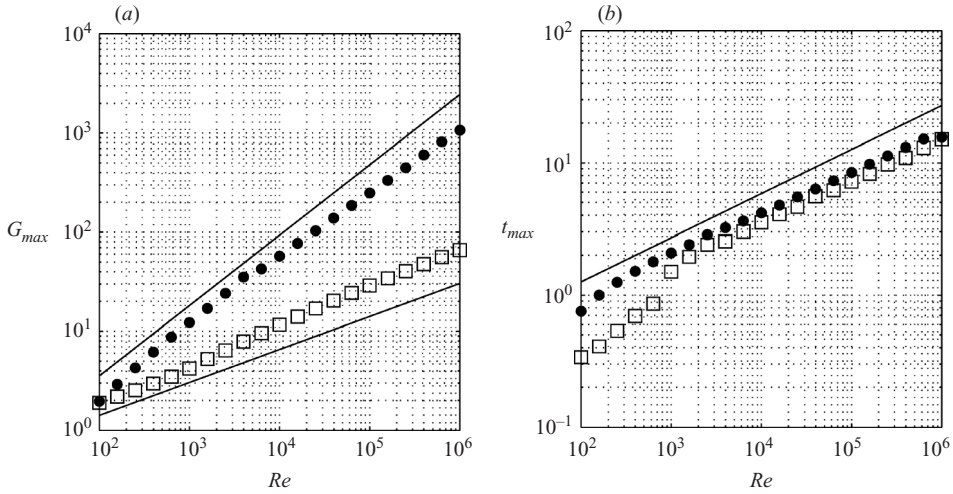
FIGURE 6. (a) Optimal gain G_{max} and (b) optimal time t_{max} for $\eta = 0.5$, $\mu = 0.5$, $Ta/Re = 18$ and $m = 1$. Circles represent $k = 0.3$, for which $\sigma = 0.07$, and squares represent $k = 1$, for which $\sigma = -0.5$. The straight lines indicate the predicted gradients (see text).

Heaton & Peake (2007) were unable to directly verify the scaling for G_{max} in (3.2) because of limitations in their numerical method; however the scaling was observed in our present computations of SPF. Figure 6 shows G_{max} for two representative cases having $Ta/Re = 18$, one for which $\sigma = 0.07$ and one for which $\sigma = -0.5$. It is clear that the two cases, which differ only by the value of the axial wavenumber, obey different scalings for G_{max} but both share the same scaling for t_{max}. The gradients of the lines in the figure indicate the scalings (3.2), and from the good level of agreement we conclude that the scalings derived by Heaton & Peake (2007) are verified. The maximum value for σ over all combinations of k, m should determine the asymptotic scaling of $\mathbb{G}$: we find that $\sigma_{max} = 0.38$ for $Ta/Re = 18$, and that σ_{max} decreases to zero as Ta/Re increases.

Although it is of some interest to give a confirmation of the scaling (3.2) conjectured by Heaton & Peake (2007), the alternative limit of $Ta \to \infty$ with Re held fixed is perhaps more important in figure 4. In this limit the mean flow approaches pure Taylor–Couette flow, but the results of Heaton & Peake (2007) can still be adapted. In this limit the quotient inside the square root in (3.3) is positive (because the numerator reduces to the Rayleigh discriminant when $U \equiv 0$), and so the maximum exponent is $\sigma_{max} = 0$, obtained by taking $k_{max} = 0$. Equations (2.1), (2.3) and (3.3) together imply that for large but finite Ta we should expect $k_{max} = O(Re/Ta)$. The final change to make is that Ta, in this limit of SPF, plays the part of the Reynolds number used by Heaton & Peake (2007). Taken together this implies the scaling:

$$\mathbb{G} \sim Ta^{2/3} \tag{3.4}$$

as $Ta \to \infty$ with Re fixed. The maximum growth in figure 4 can be seen to conform to this scaling. Further investigation of the axial wavelength in our computations also confirms that the scaling $k_{max} \propto Re/Ta$ is indeed obtained.

Figure 7 shows the visualization of an example optimal disturbance in the large-Ta regime described. For the case shown the energy gain is $\mathbb{G} = 16.5$, with $m_{max} = 3$ and $k_{max} = 4.0 \times 10^{-4}$. Throughout the evolution of the disturbance we find that the axial velocity component u is negligible. At $t = 0$ we find that 1% of the kinetic energy
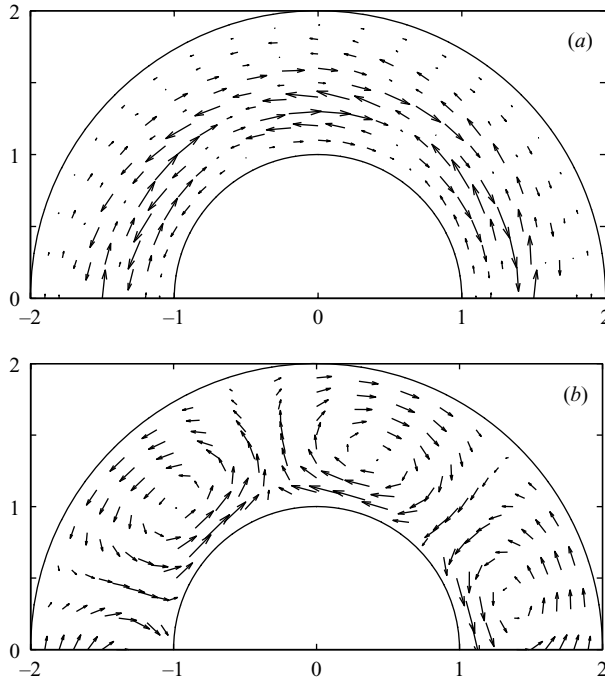
FIGURE 7. Visualizations of the optimal disturbance for $\eta = 0.5$, $\mu = 0.5$, $Re = 10$, $Ta = 10^4$. (a) $t = 0$, (b) $t = t_{max}$. Arrows indicate the cross-section velocity. The axial velocity (not shown) is negligible.

is due to v and 99% is due to w. Therefore the initial disturbance predominantly consists of azimuthal velocity perturbations, as in figure 7(a). The disturbance must however have non-zero radial velocity to satisfy continuity (2.8), and in fact v is approximately one tenth the magnitude of w. During the evolution of the disturbance the radial velocity grows in importance, so that when $t = t_{max}$ 29% of the kinetic energy is due to v, with 71% now due to w. The final state is shown in figure 7(b). The mean flow (2.1)–(2.3) is predominantly vortical, and since the axial wavenumber is small the final state of the disturbance might be termed as 'spanwise rolls'.

We have seen in this subsection how the transient growth for asymptotically stable SPF with $\mu > \eta^2$ can make a connection between two distinct regimes: the first being $\mathbb{G} \sim Re^2$ growth of streamwise disturbances when the swirl is weak, and the second being $\mathbb{G} \sim Ta^{2/3}$ growth when the axial flow is weak. We note that at large Ta in figure 4 there is no trace of the 'anti-lift-up' effect recently found by Antkowiak & Brancher (2007). This raises an interesting question of the relationship between our present SPF results and Antkowiak & Brancher's results. Antkowiak & Brancher found strong transient growth of $m = 0$ axisymmetric disturbances to a pure vortex without axial flow. The physical mechanism given by Antkowiak & Brancher (2007) for their effect requires the existence of a 'quasi-potential region' in the mean flow (i.e. $U = 0$, $W \propto 1/r$); no such region is present in the SPF in figure 4, hence the effect is not possible. The same conclusion can also be reached by adapting the mathematical arguments of § 4 of Heaton & Peake (2007): a pure vortex with $m = 0$ has no continuous spectrum so any transient growth must result from a special algebraic instability analogous to Landahl's (1980) instability. On reworking Landahl's arguments for the case of a pure vortex with $m = 0$, it is soon found that $W \propto 1/r$ is
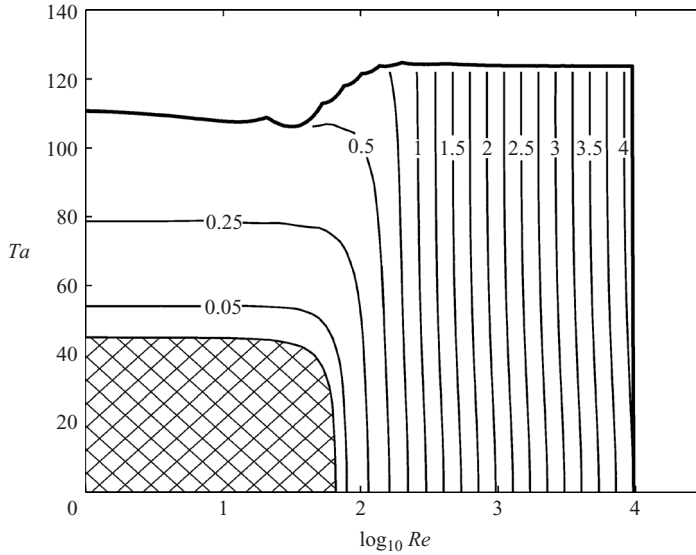
FIGURE 8. Contours of maximum transient growth $\mathbb{G}$ for $\eta = 0.5$, $\mu = -0.5$. Contour labels show the value of $\log_{10} \mathbb{G}$, in steps of 0.25 unless otherwise indicated. The thick line is the neutral curve for asymptotic linear stability. $\mathbb{G} \equiv 1$ throughout the hatched region.
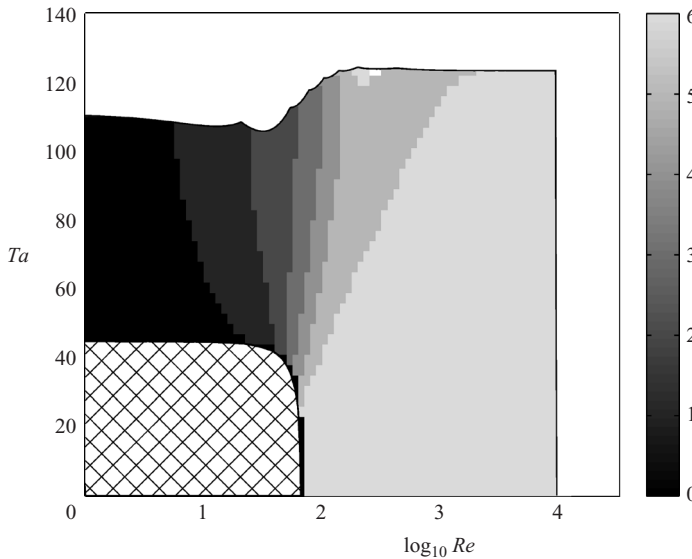
FIGURE 9. Values of m which attain the maximum transient growth for $\eta = 0.5$, $\mu = -0.5$.

required. Although this holds in the far field of a Lamb–Oseen vortex (Antkowiak & Brancher 2007), it is not true in SPF except in the special case $\mu = \eta^2$. For this special case of SPF, our calculations do show Antkowiak & Brancher's anti-lift-up effect: the $m = 0$ disturbances have $\mathbb{G} \sim Ta^2$ as $Ta \to \infty$, Re fixed.

3.3. *Counter-rotating outer cylinder* ($\mu = -0.5$)

The maximum transient growth for the case of counter-rotating cylinders with $= -0.5$ is given in figure 8, with the corresponding values of m_{max} given in figure 9. In this case

$\mu < \eta^2$ and the neutral curve reverts to the simpler form, extending from the Tollmien–Schlichting wave at $Re = 10\,359$ down to $Re = 0$. For $Re \gtrsim 100$ the optimal growth is similar to that seen in previous cases with $\mathbb{G} \sim Re^2$, $k_{max} \sim Ta/Re$ (streamwise optimal disturbances) and using the same mechanism as in Hagen–Poiseuille flow (Schmid & Henningson 1994). Like other cases, we anticipate that bypass transition will occur at large Re due to these optimal transients, and that the neutral curve will not be important.

Like the other cases a no-growth region in which $\mathbb{G} \equiv 1$ is found for small Re, Ta. The no-growth region is confined to $Ta < 44.90$, and in contrast to the $\mu = 0$ case of figure 1 there is now a substantial area above the no-growth region and beneath the neutral curve. There appears to be a general trend that for μ increasingly negative the distance between the neutral curve and the no-growth region grows, although this has not been exhaustively checked. In figure 8 the growth $\mathbb{G}$ is only modest above the no-growth region, but the flat contours suggest that the early stages of a $Ta \to \infty$ limit similar to that discussed in the previous subsection are being observed here. For $\mu \ll -1$ the larger gap between the neutral curve and no-growth region should allow significant levels of growth by the centrifugal mechanism discussed above. For such μ this raises the possibility of a centrifugal form of bypass transition at small Re. There are no experimental data available to test this possibility for SPF, but there is some related evidence from the Taylor–Couette limit ($Re = 0$). Coles (1965) reported a number of cases of transition of Taylor–Couette flow in his experiments at values of Ta significantly less than Ta_{crit}^{theo} (Coles termed this 'catastrophic transition'). These data were all for $\mu \leqslant -3.85$ and were recently investigated by Meseguer (2002), who found a strong correlation between Coles' results and the level of transient growth, and therefore conjectured a bypass transition initiated by transients as an explanation for the transition.

For an example of centrifugal transient growth when $\mu \ll -1$ we take parameters from one of Coles' experiments that was studied by Meseguer (2002), and add an additional axial mean flow (i.e. $Re \neq 0$). We take $\eta = 0.881$, $\mu = -3.85$ and $Ta = 79.8$, corresponding to the first row in table I of Meseguer (2002), and set $Re = 20$. A maximum energy gain of $\mathbb{G} = 71.8$ is found, with $m_{max} = 11$ and $k_{max} = 2.133$. As might be expected from the flat contour lines in figure 8, $\mathbb{G}$ is close to the value of 71.4 reported by Meseguer (2002) for $Re = 0$. The optimal disturbance is fully three-dimensional so a simple visualization is not possible; instead figure 10 shows the radial profiles of the three components of disturbance velocity. In the initial disturbance most of the energy is contributed by u (69%), and in the final state most of the energy (66%) is found in w. Similar energy budgets were also seen in other $\mu \ll -1$ cases we investigated. The optimal disturbance in this case has $\sigma = 0.094$, so the $Ta^{2/3}$ scaling found for $\mu > \eta^2$ in §3.2 does not hold exactly. This is because $\mu < \eta^2$ implies a negative Rayleigh discriminant inside the square root in (3.3), and so $\sigma > 0$ for $|k| > 0$. Larger $|k|$ means stronger viscous damping however, so the optimal disturbance finds a compromise at a finite wavenumber, $k_{max} = 2.133$.

In summary, centrifugal transient growth is found at small Re and large Ta, particularly for strong counter-rotation $\mu \ll -1$. For $\mu \ll -1$ it is suggested that bypass transition might be initiated by such transients for Ta less than the critical value, in a similar manner to Taylor–Couette flow (Meseguer 2002). The same possibility, bypass transition due to centrifugal transients, also exists for $\mu > \eta^2$ because then there is no critical Ta at small Re, as in figure 4.
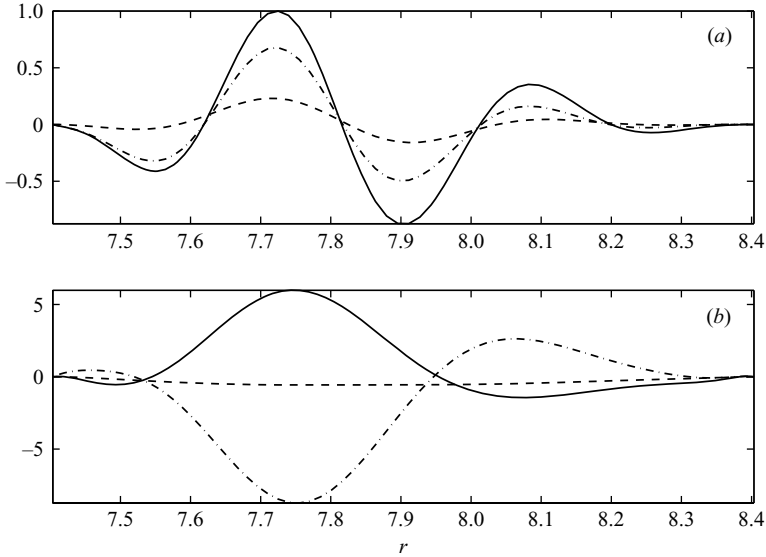
FIGURE 10. Plots of the optimal disturbance for $\eta = 0.881$, $\mu = -3.85$, $Re = 20$, $Ta = 79.8$. (*a*) $t = 0$, (*b*) $t = t_{max}$. Solid lines show u, dashed lines show v and dash-dot lines show w.

4. Transition at moderate *Re*

4.1. *Motivation*

In this section we study a model for the secondary interaction between the primary mode in SPF and the transiently growing disturbances. To motivate this, we recap the experimental data for SPF stability reviewed by Cotrell *et al.* (2004). They collate data from several experiments in which $\mu = 0$, and the experiments of Snyder (1965) and Mavec (1973) in which μ was varied. Critical values of *Ta* from experiments and from computation of the neutral curve were compared, the agreement in many cases being very good.

At low *Re* Cotrell *et al.* (2004) find that the agreement between Ta_{crit}^{expt} and Ta_{crit}^{theo} is excellent. An explanation for this is that none of the experimental data at low *Re* are for $\mu \ll -1$ or $\mu > \eta^2$, so there is no possibility of bypass transition via centrifugal transients of the type discussed at the end of §3.3. Instead the maximum transient growth $\mathbb{G}$ is small in the low-*Re* cases so transients cannot play a role in the transition, hence transition occurs directly at the neutral curve.

At high *Re* it is found that Ta_{crit}^{expt} decreases to zero at $Re = O(10^3)$ (Kaye & Elgar 1958 and Yamada 1962 find this for $\mu = 0$; there are no data for $\mu \neq 0$ but we expect that the same behaviour would result). The proposed explanation for this is that the strong transient growth of streamwise disturbances triggers bypass transition, in much the same way as is believed for other shear flows (Schmid & Henningson 2001).

At moderate *Re*, in particular in the data of Mavec (1973) at $Re = 330$ and 403.5, small but systematic discrepancies between Ta_{crit}^{expt} and Ta_{crit}^{theo} appear. For negative and small μ the transition in Mavec's data is delayed ($Ta_{crit}^{expt} > Ta_{crit}^{theo}$), whereas for larger μ the transition is subcritical ($Ta_{crit}^{expt} < Ta_{crit}^{theo}$). The systematic nature of this trend is noted by Cotrell *et al.*, who comment that "the difference $\Delta (= Ta_{crit}^{theo} - Ta_{crit}^{expt})$ at each *Re* varies nearly monotonically with μ" (Cotrell *et al.* 2004, p. 367).

The motivation for the study presented in this section is the observation that at small *Re* transition is evidently dictated purely by the primary mode and neutral curve

in Mavec's data. At larger Re transient growth levels increase, such that eventually transients are more important than the primary mode and bypass transition occurs. At moderate Re it is therefore natural to suppose that both primary mode and transient growth are simultaneously important, and hence that an explanation of the delayed/subcritical transition can be found in the optimal transients.

4.2. *Secondary instability model*

The transition mechanism at small Re is of the simplest possible type, being triggered by the linear instability of the primary mode. The model we outline here is a perturbation about this mechanism, an attempt to find the leading-order effect of small, but non-zero, amplitude transient growth. As such, our model is formally valid at values of Re which are

(*a*) small enough that instability of the primary mode is the dominant cause of transition

(*b*) large enough that a relatively small deviation of Ta_{crit}^{expt} from Ta_{crit}^{theo} is evident.
The model will be applied to the data of Mavec (1973) which are for $Re = 330$ and 403.5, which we believe satisfy these criteria.

We consider the secondary instability of a transiently growing disturbance of amplitude A, where A is real and $0 < A \ll 1$. We therefore investigate the stability of a mean flow U_0 which is an approximate (but not exact) solution of the Navier–Stokes equations having the form

$$\left. \begin{aligned} U_0(r) &= U(r) + A(U_t(r, t)e^{ik_t x + im_t \theta} + U_t^*(r, t)e^{-ik_t x - im_t \theta}), \\ V_0(r) &= 0 + A(V_t(r, t)e^{ik_t x + im_t \theta} + V_t^*(r, t)e^{-ik_t x - im_t \theta}), \\ W_0(r) &= W(r) + A(W_t(r, t)e^{ik_t x + im_t \theta} + W_t^*(r, t)e^{-ik_t x - im_t \theta}), \end{aligned} \right\} \quad (4.1)$$

where $U(r)$, $W(r)$ are given by (2.1) and (2.3). Asterisk denotes complex conjugate, and the subscript 't' denotes quantities corresponding to the transient; thus k_t and m_t are the transient's wavenumbers and U_t, V_t and W_t are its complex amplitude. We make a key approximation that the transient has saturated at amplitude A, so that it oscillates in time but does not grow or decay, and maintains a fixed shape. Thus $U_t(r, t) = U_t(r)e^{-i\lambda t}$ with λ real, and similarly for V_t and W_t.

This 'shape assumption' is standard in secondary instability theories, for example see the review in Chapter 8 of Schmid & Henningson (2001). Tollmien–Schlichting waves of course evolve with a fixed mode shape (radial profile), and for their secondary instability it is common to take λ to be the real part of the complex Tollmien–Schlichting eigenfrequency. For secondary instability of streaks in a boundary layer the radial profile is not fixed throughout the streak's evolution, but it is nevertheless found to be a suitable approximation to take the radial profile at time t_{max} together with $\lambda = 0$ (Reddy *et al.* 1998; Cossu & Brandt 2004; Cossu, Chevalier & Henningson 2007). Here too the radial profile is not fixed throughout the evolution of a transient, but similarly it is observed in calculations that the shape remains fixed to a good approximation for $t \gtrsim t_{max}/2$. We therefore take the profiles at $t = t_{max}$, when the transient achieves its maximum growth, to be the shape of the saturated disturbance in (4.1). The value for λ is taken to be the real part of the least-stable eigenfrequency in the transient. Some theoretical justification for these choices can be found in Appendix B of Heaton & Peake (2007), where a mathematical account is given of the transient growth process in swirling flow. Essentially, the optimal disturbance minimizes the amount of cancellation between eigenmodes at $t = t_{max}$ and maximizes it at $t = 0$, thereby maximizing the energy growth. The cancellations between the various

non-orthogonal eigenmodes are responsible for the non-trivial, non-modal, evolution of the disturbance, but once they are gone it is possible to approximate the transient in the manner described. We will check the validity of our assumptions *a posteriori* and find that the value for λ, in some cases, is a poor approximation. However, the results of our model are in fact remarkably robust to the exact value given to λ, so we believe that the model gives the correct qualitative trend nonetheless.

The mean flow (4.1) is inserted into the linearized Navier–Stokes equation in the form

$$\frac{\partial \boldsymbol{u}}{\partial t} + \boldsymbol{u} \cdot \nabla \boldsymbol{U}_0 + \boldsymbol{U}_0 \cdot \nabla \boldsymbol{u} = -\nabla p + \frac{1}{Re} \nabla^2 \boldsymbol{u} . \tag{4.2}$$

The resulting set of equations have coefficients periodic in x, θ and t. By a standard Floquet theory argument we may write

$$u(x, r, \theta, t) = e^{\alpha x + \beta \theta + \gamma t} \hat{u}(x, r, \theta, t) \tag{4.3}$$

where $\hat{u}$ is $2\pi/k_t$ periodic in x, $2\pi/m_t$ periodic in θ and $2\pi/\lambda$ periodic in t. The Floquet multipliers α, β and γ are free to choose. The appropriate choice to make here is to de-tune the disturbance (Schmid & Henningson 2001, p. 376) from the fundamental, i.e. the transient. In order to find the secondary effect of the transient on the primary mode, it is appropriate to set

$$\alpha = \mathrm{i} k_m, \tag{4.4}$$

$$\beta = \mathrm{i} m_m, \tag{4.5}$$

where quantities with subscript m pertain to the primary mode at the neutral curve. Using a Fourier series representation for the triply periodic function $\hat{u}(x, r, \theta, t)$, we may write

$$u(x, r, \theta, t) = e^{\mathrm{i}(k_m x + m_m \theta) + \gamma t} \sum_{a,b,c=-\infty}^{\infty} \hat{u}_{a,b,c}(r) e^{\mathrm{i}(a k_t x + b m_t \theta - c \lambda t)} . \tag{4.6}$$

A simplification is available due to the nature of the coupling between Fourier modes which occurs on substitution into (4.2): coupling only occurs between modes having $a = b = c$, hence we may take

$$u(x, r, \theta, t) = e^{\mathrm{i}(k_m x + m_m \theta) + \gamma t} \sum_{a=-\infty}^{\infty} \hat{u}_a(r) e^{\mathrm{i} a(k_t x + m_t \theta - \lambda t)} , \tag{4.7}$$

and similarly for the other components of the disturbance, v, w and p. Substituting (4.7) into (4.2) yields an infinite set of coupled equations (A1)–(A4) which are given in the Appendix. Equations (A1)–(A4) constitute an eigenvalue problem for γ, which is now the only remaining unknown quantity. In view of (4.7), the real part of γ corresponds to a temporal growth rate, so let us define the maximum growth rate over all eigenvalues as

$$\Gamma = \max \mathrm{Re}(\gamma) . \tag{4.8}$$

The coupling between equations with different values of a only occurs at $O(A)$, which is assumed to be small. When $A = 0$ it is seen that the equations are uncoupled. Indeed, when $A = 0$ equations (A1)–(A4) are precisely, for each $a \in \mathbb{Z}$, the eigenvalue problem for the frequency spectrum of SPF for axial wavenumber $k_m + a k_t$ and azimuthal wavenumber $m_m + a m_t$. By construction, since we perturb about the primary mode at the neutral curve, the most unstable mode over all k, m has zero

growth rate and occurs for $(k, m) = (k_m, m_m)$. Therefore it follows that $\Gamma = 0$ when $A = 0$.

For small but non-zero A the full eigenvalue problem for the infinite system of equations given by (A1)–(A4) must be solved. This computation is made possible by truncating the system to include only $-M \leqslant a \leqslant M$. The computation is then an eigenvalue problem of size $4N(2M + 1)$, where N is the number of radial collocation points. Because the coupling between the equations for different values of a is weak, occurring at $O(A)$, the truncation number M need not be very large. We empirically found that $M = 1$ or 2 is satisfactory to ensure numerical convergence of Γ.

Having outlined how to compute Γ by solving our secondary instability model, it is necessary to interpret this quantity in terms of SPF stability. If, for small A, it is found that $\Gamma < 0$ then we interpret this to mean that the leading-order effect of the transient on the primary mode is a stabilizing one. Therefore this should correspond to slightly delayed transition of SPF at the moderate Re we are considering in this section. Alternatively if $\Gamma > 0$ for small A, then this is to be interpreted as a destabilizing effect of the transient on the primary mode, implying slightly subcritical transition. Note that making $A \rightarrow -A$ leaves the eigenvalues γ of (A1)–(A4) unchanged (the eigenvector is multiplied by $(-1)^a$ in each component). Therefore Γ depends quadratically on the amplitude,

$$\Gamma = bA^2 + O(A^4) \tag{4.9}$$

for some real b. In summary, the proposed model for secondary instability of a transient reduces to a mathematically well-posed problem whereby we determine whether $b > 0$ or $b < 0$.

4.3. *Application of the secondary instability model*

We apply the model proposed in §4.2 to the data of Mavec (1973) having $Re = 330$ and 403.5, as reproduced in table 3 of Cotrell *et al.* (2004). First, we need to explain a few details of how the secondary instability model was applied. For each case we start with the values of η, μ and Re from Mavec's experiment. Given these values we determine Ta_{crit}^{theo}, the value of Ta on the neutral curve where the most unstable mode is neutrally stable. This, and the corresponding wavenumbers of the neutral mode are denoted as m_m, k_m and Ta_m to avoid confusion with the quantities pertaining to the transient. The neutral modes were also calculated by Cotrell *et al.* (2004), and we find that our values are in agreement with theirs, except for cases 13-14 in table 1 below and cases 10-11 in table 2 below. For these four cases it appears that Cotrell *et al.* (2004) did not include wavenumbers with $mk < 0$ in their computation. The critical value of Ta that we find is slightly lower than the value given by Cotrell *et al.* (2004) in these four cases, but in none of them does it affect the qualitative assessment of Mavec's results (subcritical transition in each of these four cases). The value of Ta_m is required for $W(r)$ in (4.1) and m_m, k_m appear in (A1)–(A4). The other quantities which are required are m_t, k_t, $U_t(r)$, $V_t(r)$, $W_t(r)$ and λ, all of which are derived from the optimal transient. At the neutral curve the definition of the optimally growing transient is complicated by the asymptotic growth of the neutral mode, so we must instead use the optimally growing transient at a slightly smaller Ta below the neutral curve. Here the definition of the optimal transient is unambiguous, and we recall from §3 that its properties vary smoothly as Ta increases towards the neutral curve. We therefore choose $Ta_t = 0.9 \times Ta_m$ for the cases in which Mavec observed delayed transition (cases 1–9 in table 1 and cases 1–7 in table 2). For the other cases, in which

		Neutral mode			Transient			Model	Mavec's
Case	μ	m_m	k_m	Ta_m	m_t	k_t	Ta_t	prediction	experiment
1	−0.82	21	3.544	74.486	18	2.80	67.04	Delayed	Delayed
2	−0.67	21	3.189	71.047	12	0.303	63.94	Delayed	Delayed
3	−0.35	20	2.438	64.454	13	0.317	58.01	Delayed	Delayed
4	−0.18	20	2.125	61.355	13	0.309	55.22	Delayed	Delayed
5	−0.071	20	1.925	59.585	13	0.311	53.63	Delayed	Delayed
6	0	20	1.816	58.536	14	0.397	52.68	Delayed	Delayed
7	0.079	19	1.613	57.427	14	0.427	51.68	Delayed	Delayed
8	0.15	19	1.509	56.531	14	0.476	50.88	Delayed	Delayed
9	0.27	19	1.344	55.325	16	1.01	49.79	Delayed	Delayed
10	0.45	18	1.050	54.274	17	1.08	52.96	Marginal	Subcritical
11	0.67	17	0.7584	55.477	16	0.876	50.17	Marginal	Subcritical
12	0.80	16	0.6094	58.996	16	0.8354	51.79	Marginal	Subcritical
13	0.96	15	−0.5188	67.565	17	−0.748	56.35	Subcritical	Subcritical
14	1.11	14	−0.4906	74.504	16	−0.705	61.94	Subcritical	Subcritical

TABLE 1. Secondary instability results for the model and the data of Mavec (1973)
with $\eta = 0.77$, $Re = 330$.

Mavec observed subcritical transition, we have used $Ta_t = Ta_{crit}^{expt}$ corresponding to the value of Ta at which transition occurred in the experiment.

In all cases we find that the precise choice of Ta_t does not change the final outcome. Similarly, the effect of varying the value of λ was tested and the results were robust to this also. The definition of λ is the weakest link in the model proposed in §4.2 because the transiently growing disturbances necessarily do not oscillate with a single frequency. Nevertheless, the validity of the approximation we make can be tested by taking a fast Fourier transform of the temporally evolving transient. For the cases with $\mu > 0$ we find that the approximation satisfactorily describes the evolution of the transient for $t \simeq t_{max}$. For the cases with $\mu \leqslant 0$ the fit is poor, and empirically it was seen that $\lambda = 0$ would be a more appropriate modelling assumption. To this end we have repeated the secondary instability calculations for all cases using $\lambda = 0$, and also for other values of λ in a selection of the cases: we found that the qualitative result was unchanged in all cases. This robustness of the results to the exact value of λ is reassuring, and suggests that the qualitative trend in the results is genuine, despite the weakness of this modelling assumption.

4.4. Results for delayed/subcritical transition

The results are given in tables 1 and 2, in which the final two columns respectively give the transition scenario predicted by the model described in §4.2, and the transition observed in Mavec's experiment. A prediction of delayed transition is made when we find that $b < 0$ in (4.9), meaning that the optimally growing transient has a secondary stabilizing effect on the primary mode. Conversely if $b > 0$ then a prediction of subcritical transition is made. Tables 1 and 2 show that the correct qualitative trend exists in the results, namely that transition is delayed for the smaller-μ data and subcritical for the larger-μ data. The nature of the changeover between the two is not clear cut, however, in the context of our simple model. For this reason some of the data are labelled as 'marginal', as we now explain.

In the case of the smaller-μ data for which the prediction is delayed transition, both the neutral mode and the transient have $mk > 0$, which we term co-rotating (because the phase velocity follows the path of a right-handed helix). In the case of

Case	μ	Neutral mode			Transient			Model prediction	Mavec's experiment
		m_m	k_m	Ta_m	m_t	k_t	Ta_t		
1	−0.63	22	2.681	71.053	12	0.236	63.95	Delayed	Delayed
2	−0.39	21	2.137	65.704	13	0.264	59.13	Delayed	Delayed
3	−0.29	21	1.975	63.669	13	0.256	57.30	Delayed	Delayed
4	−0.13	20	1.662	60.717	13	0.249	54.65	Delayed	Delayed
5	0	20	1.481	58.555	14	0.313	52.70	Delayed	Delayed
6	0.097	20	1.359	57.179	14	0.337	51.46	Delayed	Delayed
7	0.2	19	1.172	55.869	15	0.553	50.28	Delayed	Delayed
8	0.72	16	0.5500	56.044	16	0.7168	47.82	Marginal	Subcritical
9	0.84	16	0.500	60.296	17	−0.6416	48.85	Subcritical	Subcritical
10	1.01	15	−0.425	68.947	16	−0.609	55.32	Subcritical	Subcritical
11	1.24	12	−0.4100	71.919	15	−0.5835	61.64	Subcritical	Subcritical

TABLE 2. Secondary instability results for the model and the data of Mavec (1973) with $\eta = 0.77$, $Re = 403.5$.
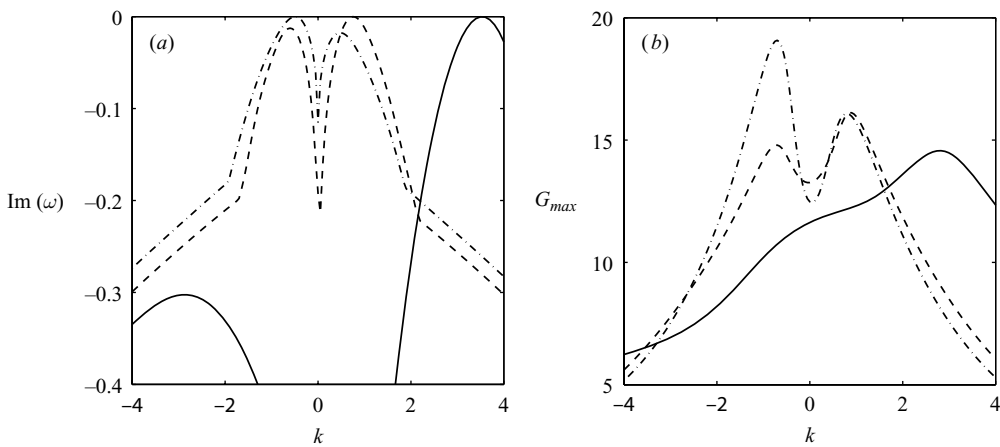

FIGURE 11. Plots as functions of k of (a) $Im(\omega)$, the primary mode growth rate, and (b) G_{max}, the maximum transient growth. Parameter values are taken from table 1 for case 1 (solid line), case 11 (dashed line) and case 14 (dash-dot line).

the larger-μ data for which the prediction is subcritical transition, counter-rotating disturbances ($mk < 0$) are prevalent. The underlying trend we observe is that the co-rotating optimal transients have a stabilizing action on the primary mode, whereas counter-rotating transients destabilize the primary mode. The changeover between these two scenarios is amplitude dependent, and hence is not precisely defined in our simple model. The cases labelled as 'marginal' in tables 1 and 2 do show a stabilizing effect of the optimal transient on the most unstable (i.e. neutral) primary mode, both of which are co-rotating. However, they also have combinations of slightly sub-optimal disturbances which are counter-rotating and which show a destabilizing effect. Whether or not destabilization involving sub-optimal modes or transients overcomes stabilization of the neutral mode by the optimal transient depends on the amplitude, and hence could vary between experiments. For this reason the prediction of the model is termed 'marginal'. Figure 11 demonstrates the nature of the changeover by displaying the primary mode growth rate ($Im(\omega)$) and the maximum transient growth as functions of k for three cases taken from table 1. In case 1 there is a single

maximum of G_{max} whose effect is to stabilize the neutral mode, so the prediction is unambiguously delayed transition. In case 14 the optimal transient destabilizes the neutral mode, so the prediction is unambiguously subcritical transition. In case 11 the optimal transient stabilizes the neutral mode, but the optimal corresponding to the $k < 0$ local maximum of G_{max} destabilizes the weakly damped primary mode corresponding to the $k < 0$ local maximum of $Im(\omega)$. This case is therefore termed marginal in table 1.

Overall our results do recover the correct trend for the delayed and subcritical transition observed experimentally by Mavec (1973). The changeover between the two scenarios is not well resolved by our simple model, but does occur at about the right values of μ. The results show a reassuring level of robustness to changes in the modelling assumptions, specifically the values of λ and Ta_t. Of course, it is possible to envisage more sophisticated models for the effect of finite-amplitude transients on the stability of SPF. In order to remove the approximation that the transient oscillates at a single frequency one could fully solve the linearized Navier–Stokes equations for the time evolution of the transient. This however has the drawback that simple Floquet analysis can no longer be used, forcing a full numerical solution of the secondary stability equations instead of the simple eigenvalue problem needed here. Such a procedure would be scarcely simpler than a full DNS computation, which would remove all the modelling assumptions. However, one attraction of the model proposed in this section is its simplicity, since an aim of the modelling process is to simplify the problem as far as validly possible.

5. Conclusions

The central results of the present paper are the computations of maximum transient growth in SPF given in § 3. We have found the maximum growth over all time t and all wavenumbers m, k throughout the stable regions of the (Re, Ta)-plane for three test cases. The test cases were chosen to coincide with those used by Cotrell & Pearlstein (2004), who computed the complete neutral curves for asymptotic linear stability of SPF. The transient growth results are complementary to knowledge of the neutral curve, and the two taken together allow an improved understanding of the linear stability of SPF.

We found that transient growth is small when Re and Ta are both small, and we infer from this that transition should occur by a classical linear instability route. This is consistent with experimental data (Cotrell *et al.* 2004), which show transition occurring at the neutral curve location. For large Re, of the order of 1000, the transient growth is large in all cases. Streamwise optimal disturbances (with $k \propto Ta/Re$) follow the usual 'roll→streak' mechanism for transient growth in parallel shear flow (Schmid & Henningson 2001) and have $\mathbb{G} \sim Re^2$. We infer that a bypass transition is probably initiated by these transients, which is consistent with experimental data (although these are only available for $\mu = 0$). Large transient growth is also seen for large Ta, which can be asymptotically stable in flows with $\mu \ll -1$ or $\mu > \eta^2$. In this regime the transient growth is centrifugal and follows the different scalings (3.2)–(3.3). Our results include the first direct numerical verification (figure 6) of the centrifugal regime scalings, and we noted that for SPF with $\mu > \eta^2$ they simplify to $\mathbb{G} \sim Ta^{2/3}$, as $Ta \to \infty$ with Re held fixed. It is suggested that these centrifugal transients might trigger a different sort of bypass transition at large Ta, small Re, in cases with $\mu \ll -1$ or $\mu > \eta^2$. This suggestion is in agreement with a recent analysis by Meseguer (2002) of some experiments by Coles (1965) at $Re = 0$, i.e. the Taylor–Couette limit, but there are no SPF data with which to compare.

For moderate *Re*, of the order of a few hundred, we have attempted to explain the delayed and subcritical transition seen in experiments (Mavec 1973; Cotrell *et al.* 2004) by proposing a simple secondary instability model. These *Re* are sufficiently small that the primary mode is the main cause of transition, but just large enough that transient growth might begin to have an effect. The model attempts to find the leading-order effect of a saturated transient on the primary mode by using Floquet theory. The results show good qualitative agreement with the experimental data, with delayed transition being favoured for negative and small μ and subcritical transition favoured for larger μ. While the results are very suggestive, they do not prove that interaction with transients is indeed the mechanism at play in the experiments and other explanations, such as the aspect ratio of the experimental annuli, have been suggested in the past (Takeuchi & Jankowski 1981; Cotrell *et al.* 2004). Nevertheless, the model in §4 gives one possible systematic explanation for the trend in Mavec's experimental data.

Overall, the transient growth is seen to exhibit two very different regimes in SPF: one dominated by the 'lift-up' mechanism seen in parallel shear flows and a second dominated by swirling flow continuous-spectrum theory (Heaton & Peake 2007). This is unsurprising since SPF is known to exhibit both shear- and centrifugal-type instabilities, which is one reason why SPF is of scientific interest as a canonical flow. The existence of the shear and centrifugal regimes, and the connection between them, has a direct analogue in the stability of the primary mode (Meseguer & Marques 2002; Cotrell & Pearlstein 2004) and is a key feature of SPF.

Appendix. Secondary instability equations

The secondary instability equations arise from substituting (4.1) and (4.7) into (4.2). The following infinite set of equations, for all $a \in \mathbb{Z}$, results:

$$(\gamma - \mathrm{i}a\lambda)\hat{u}_a + U'\hat{v}_a + \left(U\mathrm{i}(k_m + ak_t) + W\frac{\mathrm{i}(m_m + am_t)}{r}\right)\hat{u}_a + \mathrm{i}(k_m + ak_t)\hat{p}_a$$

$$- \frac{1}{Re}\left(\hat{u}_a'' + \frac{\hat{u}_a'}{r} - \frac{(m_m + am_t)^2}{r^2}\hat{u}_a - (k_m + ak_t)^2\hat{u}_a\right)$$

$$= -A\left\{\mathrm{i}k_t U_t\hat{u}_{a-1} + U_t'\hat{v}_{a-1} + U_t\frac{\mathrm{i}m_t}{r}\hat{w}_{a-1} - \mathrm{i}k_t U_t^*\hat{u}_{a+1} + U_t'^*\hat{v}_{a+1} - U_t^*\frac{\mathrm{i}m_t}{r}\hat{w}_{a+1}\right.$$

$$+ U_t\mathrm{i}(k_m + (a-1)k_t)\hat{u}_{a-1} + V_t\hat{u}_{a-1}' + W_t\frac{\mathrm{i}(m_m + (a-1)m_t)}{r}\hat{u}_{a-1}$$

$$\left. + U_t^*\mathrm{i}(k_m + (a+1)k_t)\hat{u}_{a+1} + V_t^*\hat{u}_{a+1}' + W_t^*\frac{\mathrm{i}(m_m + (a+1)m_t)}{r}\hat{u}_{a+1}\right\}, \tag{A1}$$

$$(\gamma - \mathrm{i}a\lambda)\hat{v}_a + \left(U\mathrm{i}(k_m + ak_t) + W\frac{\mathrm{i}(m_m + am_t)}{r}\right)\hat{v}_a + \hat{p}_a'$$

$$- \frac{1}{Re}\left(\hat{v}_a'' + \frac{\hat{v}_a'}{r} - \frac{\hat{v}_a}{r^2} - \frac{(m_m + am_t)^2}{r^2}\hat{v}_a - (k_m + ak_t)^2\hat{v}_a - \frac{2\mathrm{i}(m_m + am_t)}{r^2}\hat{w}_a\right)$$

$$= -A\left\{\mathrm{i}k_t V_t\hat{u}_{a-1} + V_t'\hat{v}_{a-1} + V_t\frac{\mathrm{i}m_t}{r}\hat{w}_{a-1}\right.$$

$$-\mathrm{i}k_t V_t^* \hat{u}_{a+1} + V_t'^* \hat{v}_{a+1} - V_t^* \frac{\mathrm{i}m_t}{r}\hat{w}_{a+1} - 2\frac{V_t}{r}\hat{v}_{a-1} - 2\frac{V_t^*}{r}\hat{v}_{a+1}$$

$$+ U_t\mathrm{i}(k_m + (a-1)k_t)\hat{v}_{a-1} + V_t\hat{v}'_{a-1} + W_t\frac{\mathrm{i}(m_m + (a-1)m_t)}{r}\hat{v}_{a-1}$$

$$+ U_t^*\mathrm{i}(k_m + (a+1)k_t)\hat{v}_{a+1} + V_t^*\hat{v}'_{a+1} + W_t^*\frac{\mathrm{i}(m_m + (a+1)m_t)}{r}\hat{v}_{a+1}\Bigg\}, \tag{A2}$$

$$(\gamma - \mathrm{i}a\lambda)\hat{w}_a + W'\hat{v}_a + \frac{W\hat{v}_a}{r} + \left(U\mathrm{i}(k_m + ak_t) + W\frac{\mathrm{i}(m_m + am_t)}{r}\right)\hat{w}_a$$

$$+ \frac{\mathrm{i}(m_m + am_t)}{r}\hat{p}_a - \frac{1}{Re}\left(\hat{w}''_a + \frac{\hat{w}'_a}{r} - \frac{\hat{w}_a}{r^2} - \frac{(m_m + am_t)^2}{r^2}\hat{w}_a\right.$$

$$\left. - (k_m + ak_t)^2\hat{w}_a + \frac{2\mathrm{i}(m_m + am_t)}{r^2}\hat{v}_a\right)$$

$$= -A\left\{\mathrm{i}k_t W_t \hat{u}_{a-1} + W'_t\hat{v}_{a-1} + W_t\frac{\mathrm{i}m_t}{r}\hat{w}_{a-1}\right.$$

$$-\mathrm{i}k_t W_t^*\hat{u}_{a+1} + W_t'^*\hat{v}_{a+1} - W_t^*\frac{\mathrm{i}m_t}{r}\hat{w}_{a+1} + \frac{V_t}{r}\hat{w}_{a-1} + \frac{V_t^*}{r}\hat{w}_{a+1}$$

$$+ U_t\mathrm{i}(k_m + (a-1)k_t)\hat{w}_{a-1} + V_t\hat{w}'_{a-1} + W_t\frac{\mathrm{i}(m_m + (a-1)m_t)}{r}\hat{w}_{a-1}$$

$$+ U_t^*\mathrm{i}(k_m + (a+1)k_t)\hat{w}_{a+1} + V_t^*\hat{w}'_{a+1} + W_t^*\frac{\mathrm{i}(m_m + (a+1)m_t)}{r}\hat{w}_{a+1}$$

$$+ \frac{W_t}{r}\hat{v}_{a-1} + \frac{W_t^*}{r}\hat{v}_{a+1}\Bigg\} \tag{A3}$$

$$\hat{v}'_a + \frac{\hat{v}_a}{r} + \frac{\mathrm{i}(m_m + am_t)}{r}\hat{w}_a + \mathrm{i}(k_m + ak_t)\hat{u}_a = 0 \tag{A4}$$

REFERENCES

ANTKOWIAK, A. & BRANCHER, P. 2004 Transient growth for the Lamb-Oseen vortex. *Phys Fluids* **16** (1), L1–L4.

ANTKOWIAK, A. & BRANCHER, P. 2007 On vortex rings around vortices: an optimal mechanism. *J. Fluid Mech.* **578**, 295–304.

BUTLER, K. M. & FARRELL, B. F. 1992 Three-dimensional optimal perturbations in viscous shear flow. *Phys Fluids* A **4**, 1637–1650.

CHANDRASEKHAR, S. 1962 The stability of spiral flow between rotating cylinders. *Proc. R. Soc. Lond.* A **265**, 188–197.

COLES, D. 1965 Transition in circular Couette flow. *J. Fluid Mech* **21**, 385–425.

COSSU, C. & BRANDT, L. 2004 On Tollmien–Schlichting-like waves in streaky boundary layers. *Eur. J. Mech.* B/*Fluids* **23**, 815–833.

COSSU, C., CHEVALIER, M. P. & HENNINGSON, D. S. 2007 Optimal secondary energy growth in a plane channel flow. *Phys Fluids* **19**, 058107.

COTRELL, D. L. & PEARLSTEIN, A. J. 2004 The connection between centrifugal instability and Tollmien–Schlichting-like instability for spiral Poiseuille flow. *J. Fluid Mech.* **509**, 331–351.

COTRELL, D. L. & PEARLSTEIN, A. J. 2006 Linear stability of spiral and annular Poiseuille flow for small radius ratio. *J. Fluid Mech.* **547**, 1–20.

COTRELL, D. L., RANI, S. L. & PEARLSTEIN, A. J. 2004 Computational assessment of subcritical and delayed onset in spiral Poiseuille flow experiments. *J. Fluid Mech.* **509**, 353–378.

DIPRIMA, R. C. 1960 The stability of a viscous fluid between rotating cylinders with an axial flow. *J. Fluid Mech.* **9**, 621–631.

DiPrima, R. C. & Swinney, H. L. 1985 Instabilities and transition in flow between concentric rotating cylinders. In *Hydrodynamic Instabilities and the Transition to Turbulence*, 2nd edn (ed. H. L. Swinney & J. P. Gollub), pp. 139–180. Springer.

Goldstein, S. 1937 The stability of viscous fluid flow between rotating cylinders. *Proc. Camb. Phil. Soc.* **33**, 41–61.

Gustavsson, L. H. 1991 Energy growth of three-dimensional disturbances in plane Poiseuille flow. *J. Fluid Mech.* **224**, 241–260.

Heaton, C. J. 2007 Optimal growth of the Batchelor vortex viscous modes. *J. Fluid Mech.* **592**, 495–505.

Heaton, C. J. & Peake, N. 2006 Algebraic and exponential instability of inviscid swirling flow. *J. Fluid Mech.* **565**, 279–318.

Heaton, C. J. & Peake, N. 2007 Transient growth in vortices with axial flow. *J. Fluid Mech.* **587**, 271–301.

Hristova, H., Roch, S., Schmid, P. J. & Tuckerman, L. S. 2002 Transient growth in Taylor–Couette flow. *Phys Fluids* **14**, 3475–3484.

Kaye, J. & Elgar, E. C. 1958 Modes of adiabatic and diabatic fluid flow in an annulus with an inner rotating cylinder. *Trans ASME* **80**, 753–765.

Landahl, M. T. 1980 A note on an algebraic instability of inviscid parallel shear flows. *J. Fluid Mech.* **98**, 243–251.

Leibovich, S. & Stewartson, K. 1983 A sufficient condition for the instability of columnar vortices. *J. Fluid Mech.* **126**, 335–356.

Mavec, J. A. 1973 Spiral and toroidal secondary motions in swirling flows through an annulus at low Reynolds numbers. MS thesis, Illinois Inst. Tech., Chicago.

Meseguer, Á. 2002 Energy transient growth in the Taylor–Couette problem. *Phys Fluids* **14**, 1655–1660.

Meseguer, A. & Marques, F. 2002 On the competition between centrifugal and shear instability in spiral Poiseuille flow. *J. Fluid Mech* **455**, 129–148.

Meseguer, A. & Marques, F. 2005 On the stability of medium gap corotating spiral Poiseuille flow. *Phys Fluids* **17**, 094104.

Ng, B. S. & Turner, E. R. 1982 On the linear stability of spiral flow between cylinders. *Proc. R. Soc. Lond.* A **382**, 83–102.

Pradeep, D. S. & Hussain, F. 2006 Transient growth of perturbations in a vortex column. *J. Fluid Mech.* **550**, 251–288.

Reddy, S. C., Schmid, P. J., Baggett, J. S. & Henningson, D. S. 1998 On the stability of streamwise streaks and transition thresholds in plane channel flows. *J. Fluid Mech.* **365**, 269–303.

Reid, W. H. 1961 Review of "The hydrodynamic stability of viscid flow between coaxial cylinders" by S. Chandrasekhar (*Proc. Natl Acad. Sci. USA* **46**, 141–143, 1960). *Math. Rev.* **22**, 565.

Schmid, P. J. & Henningson, D. S. 1994 Optimal energy density growth in Hagen-Poiseuille flow. *J. Fluid Mech.* **277**, 197–225.

Schmid, P. J. & Henningson, D. S. 2001 *Stability and Transition in Shear Flows*. Springer.

Snyder, H. A. 1965 Experiments on the stability of two types of spiral flow. *Ann. Phys* **31**, 292–313.

Synge, J. L. 1938 On the stability of a viscous liquid between rotating coaxial cylinders. *Proc. R. Soc. Lond.* A **167**, 250–256.

Takeuchi, D. I. & Jankowski, D. F. 1981 A numerical and experimental investigation of the stability of spiral Poiseuille flow. *J. Fluid Mech.* **102**, 101–126.

Taylor, G. I. 1923 Stability of a viscous liquid contained between two rotating cylinders. *Phil. Trans R. Soc. Lond.* A **223**, 289–343.

Trefethen, L. N., Trefethen, A. E., Reddy, S. C. & Driscoll, T. A. 1993 Hydrodynamic stability without eigenvalues. *Science* **261**, 578–584.

Yamada, Y. 1962 Resistance of a flow through an annulus with an inner rotating cylinder. *Bull. JSME* **5**, 302–310.